Basic dye decomposition kinetics in a photocatalytic slurry reactor

Chun-Hsing Wu, Hung-Wei Chang, Jia-Ming Chern *

Department of Chemical Engineering, Tatung University, 40 Chungshan North Road, 3rd Sec., Taipei 10452, Taiwan

Abstract

Wastewater effluent from textile plants using various dyes is one of the major water pollutants to the environment. Traditional chemical, physical and biological processes for treating textile dye wastewaters have disadvantages such as high cost, energy waste and generating secondary pollution during the treatment process. The photocatalytic process using TiO_2 semiconductor particles under UV light illumination has been shown to be potentially advantageous and applicable in the treatment of wastewater pollutants. In this study, the dye decomposition kinetics by nano-size TiO_2 suspension at natural solution pH was experimentally studied by varying the agitation speed (50–200 rpm), TiO_2 suspension concentration (0.25–1.71 g/L), initial dye concentration (10–50 ppm), temperature (10–50 °C), and UV power intensity (0–96 W). The experimental results show the agitation speed, varying from 50 to 200 rpm, has a slight influence on the dye decomposition rate and the pH history; the dye decomposition rate increases with the TiO_2 suspension concentration up to 0.98 g/L, then decrease with increasing TiO_2 suspension concentration; the initial dye decomposition rate increases with the initial dye concentration up to a certain value depending upon the temperature, then decreases with increasing initial dye concentration; the dye decomposition rate increases with the UV power intensity up to 64 W to reach a plateau. Kinetic models have been developed to fit the experimental kinetic data well.
© 2006 Elsevier B.V. All rights reserved.

1. Introduction

Wastewater effluent from textile plants using various dyes is one of the major water pollutants to the environment. Except for coloring the receiving water bodies such as rivers and lakes, dyes in the water bodies also undergo chemical and biological changes that consume dissolved oxygen in the water bodies. Some dyes even possess toxicity that is hazardous to aquatic life. Traditional methods for treating the textile dye wastewaters consist of various chemical, physical, and biological processes. For example, Liu et al. [1] investigated the treatment of direct dye wastewater by coagulation; Sanghi and Bhattacharya [2] studied the adsorption–coagulation for the decolorisation of textile dye solutions; Beydilli et al. [3] reported the possibility of decolorization of azo dye biologically under aerobic, anoxic, and methanogenic conditions. Liakou et al. [4] studied a combined chemical and biological treatment of wastewater containing azo dyes. They first used ozonation processes to decompose the refractory substrates in the stream, and then used biological treatment to detoxify the benzen-sulfonate produced in the ozonation step.

More advanced treatment processes include adsorption, electrocoagulation, ultrasonic decomposition, advanced chemical oxidation, nanofiltration, chemical coagulation followed by sedimentation and so forth. According to the research of Van der Bruggen et al. [5], three nanofiltration membranes were possible to treat four different types of textile dye wastewater, but the color removal efficiency by the membranes was lower than that of biological treatment. Koyuncu [6] studied the treatment and reuse of both synthetic and industrial dyes by nanofiltration membranes. Ge and Qu [7] investigated the degradation of azo dye Acid Red B on MnO_2 enhanced by ultrasonic irradiation.

Since most of the above dye treatment methods have disadvantages such as high cost and generating secondary pollution during the treatment process, advanced oxidation processes (AOPs) involving hydroxyl radical are introduced to treat textile dyes effluents [8–11]. Among the many AOPs, the most efficient and economical method is probably the photocatalysis by TiO_2/UV. Due to the advantages of photocatalytic decomposition of organic pollutants using TiO_2 particles or films,

* Corresponding author. Tel.: +886 2 27002737x23; fax: +886 2 27087819.
E-mail address: jmchern@ttu.edu.tw (J.-M. Chern).

advanced oxidation by TiO_2/UV has been gaining industrial and academic attention. However, most studies investigate only some, not all factors that might influence the degradation rate of organic compounds in aqueous systems [12–15]. This study therefore aims at studying the dye decomposition kinetics in a batch photocatalytic reactor under various operating conditions including agitation speed, TiO_2 suspension concentration, initial dye concentration, temperature, and UV illumination intensity in attempt to establish reaction kinetic models that can be used for process design and optimization.

2. Experimental

2.1. Materials

The basic dye (1000 mg/L solution pH 9.28 at 25 °C), HF6 coral pink with the main ingredient of triphenyalmethane (Taipei First Chemical Company, Taiwan) was directly used without further purification. Fig. 1 shows the UV absorbance spectrum of the dye solution. The TiO_2 suspension (Tatung Fine Chemicals Company, Taiwan) has pH 7.5 at 25 °C and its UV absorbance spectrum is also shown in Fig. 1. The TiO_2 suspension has solid content 15 wt.%, density 1.22 g/mL, and the TiO_2 crystalline phase is anatase. The particle size distribution of the TiO_2 suspension measured by a dynamic light scattering analyzer (HORIBA LB-500, Japan) results in 95% particle size less than 30 nm and mean particle size 19.8 nm.

2.2. Apparatus

Fig. 2 schematically shows the jacketed photocatalytic reactor system (Jyi Goang, Taiwan). The reactor is made of stainless steel equipped with a 20 W DC motor that controls the agitating speed at the desired level. Twelve sets of 365 nm, 8 W UV lamps (Sankyo, Japan) were used; the ON/OFF status of each lamp could be independently controlled. A pH monitoring
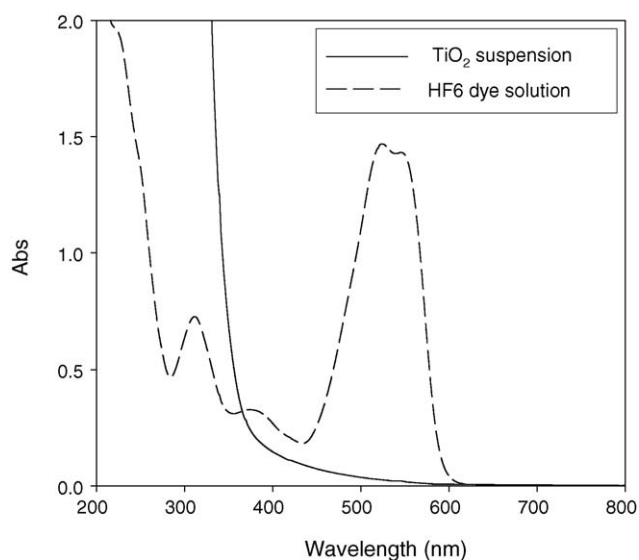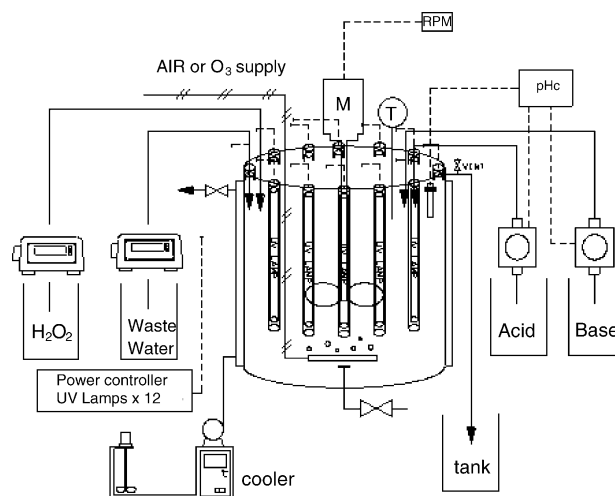

Fig. 2. Schematic diagram of the photocatalytic reactor system.

and controlling system was used to monitor the pH history during reaction. A temperature control system (Water Bath D-630, Deng Yng, Taiwan) was used to control the reaction temperature at desired level.

2.3. Procedures

First of all, 15 L deionized water was charged to the photocatalytic reactor and the agitating and temperature control system were turned on. The desired amount of TiO_2 suspension was added to the reactor and mixed with the deionized water for 5 min, then a sample was taken as the reference. The dye solution with the desired initial concentration was added to the photocatalytic reactor and mixed with the TiO_2 suspension for 15 min, and then another sample was taken. Upon adding the dye solution, the pH monitoring system was started without controlling the solution pH during reaction. The UV light was turned on and the dye solution samples were taken at the desired time intervals. After filtration, the dye solution samples were analyzed by an UV/vis Spectrophotometer (Jasco V-560, Japan) at $\lambda_{max} = 523$ nm with a calibration curve based on the Beer–Lambert's law. As shown in Fig. 1, the absorbance of TiO_2 suspension solution occurs at the wavelength less than 400 nm; hence the existence of TiO_2 does not interfere the dye concentration measured at the wavelength at 523 nm. The operating conditions of all experimental test runs are summarized in Table 1.

3. Results and discussions

3.1. Effect of agitation speed

The first series of experimental tests performed in this study is to vary the agitation speed while keeping all other factors constant. Fig. 3 shows a typical unsteady-state dye concentration and solution pH versus time. As shown in Fig. 3, the dye concentration almost decreases linearly with time, the solution pH also decreases with time but the relationship is not linear. When

Fig. 1. UV absorbance spectrum of the TiO_2 suspension and HF6 dye solution.

Table 1
Operating conditions of all experimental test runs

| Run no.	N (rpm)	TiO_2 (g/L)	Dye (mg/L)	UV (W)	Temp. (°C)
1	100	0.49	20	32	25
2	200	0.49	20	32	25
3	50	0.49	20	32	25
4	150	0.49	20	32	25
5	150	0.25	20	32	25
6	150	0.73	20	32	25
7	150	0.98	20	32	25
8	150	1.22	20	32	25
9	150	1.47	20	32	25
10	150	1.71	20	32	25
11	150	1.22	10	32	25
12	150	1.22	30	32	25
13	150	1.22	40	32	25
14	150	1.22	50	32	25
15	150	1.22	20	64	25
16	150	1.22	20	96	25
17	150	1.22	20	16	25
18	150	1.22	20	0	25
19	150	1.22	20	32	50
20	150	1.22	20	32	10
21	150	1.22	20	32	40
22	150	1.22	10	32	35
23	150	1.22	20	32	35
24	150	1.22	30	32	35
25	150	1.22	40	32	35
26	150	1.22	50	32	35
27	150	1.22	10	32	15
28	150	1.22	20	32	15
29	150	1.22	30	32	15
30	150	1.22	40	32	15
31	150	1.22	50	32	15
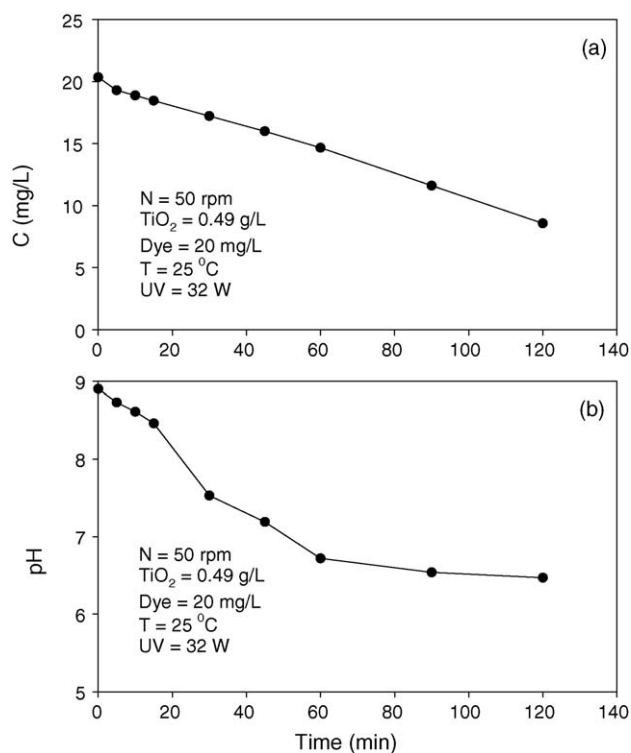
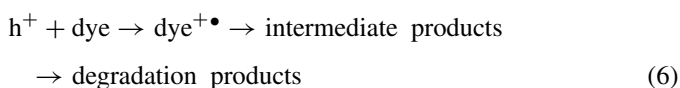Fig. 3. Dye concentration and pH histories at 50-rpm agitation speed.
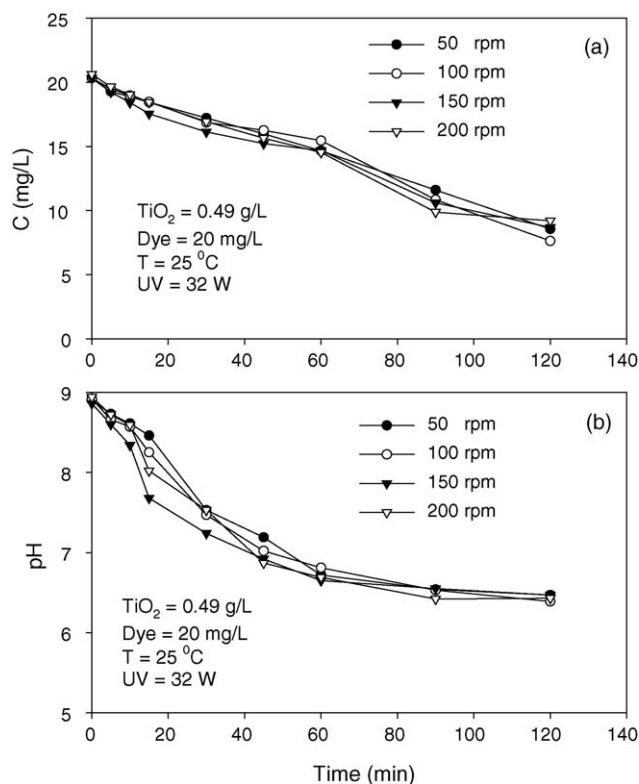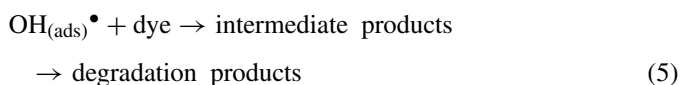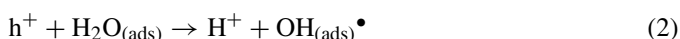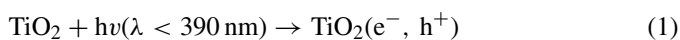

Fig. 4. Effects of agitation speed on the dye concentration and pH histories.

the dye solution was irradiated in the presence of TiO_2 photocatalyst, the adsorbed water molecules reacted with the holes in the valence band to form hydroxyl radicals and release hydrogen ions. Furthermore, the dye molecules might be decomposed to form organic acids as the intermediate products [16–18]:

$$TiO_2 + h\upsilon(\lambda < 390\,nm) \rightarrow TiO_2(e^-, h^+) \tag{1}$$

$$h^+ + H_2O_{(ads)} \rightarrow H^+ + OH_{(ads)}^\bullet \tag{2}$$

$$h^+ + OH_{(ads)}^- \rightarrow OH_{(ads)}^\bullet \tag{3}$$

$$e^- + O_{2(ads)} \rightarrow O_2^{-\bullet} \tag{4}$$

$$OH_{(ads)}^\bullet + dye \rightarrow intermediate\ products$$
$$\rightarrow degradation\ products \tag{5}$$

$$h^+ + dye \rightarrow dye^{+\bullet} \rightarrow intermediate\ products$$
$$\rightarrow degradation\ products \tag{6}$$

Those two mechanisms probably explain why the solution pH decreases during the reaction period. It is important to note that no new UV/vis peaks appeared in the dye solution samples at varying reaction times. This reveals either the life times of the intermediate products during dye decomposition are very short or the intermediate products do not absorb the UV/vis. In order to elucidate the detailed reaction pathway and to obtain a more comprehensive kinetic model, the intermediate products should be determined by other instruments such as HPLC.
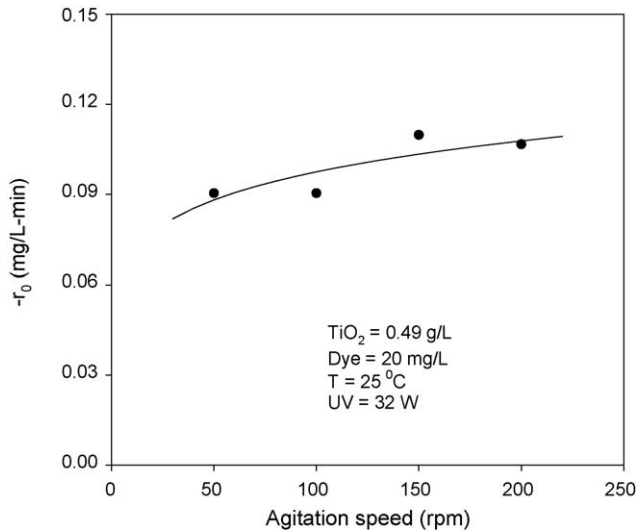
Fig. 5. Effects of agitation speed on the dye initial decomposition rate.

Fig. 6. Effects of TiO$_2$ concentration on the dye concentration history.

Fig. 4 summarizes and shows the effects of agitation speed on the dye concentration and solution pH histories. The initial reaction rates at varying agitation speeds are computed from the initial slopes and the results are shown in Fig. 5 from which we can conclude that the dye decomposition rate slightly increases with the agitation speed. For any chemical reaction influenced by mass transfer, the overall rate resistance is the summation of the mass-transfer resistance and the chemical reaction resistance:

$$\frac{1}{k} = \frac{1}{k_c} + \frac{1}{k_r} \qquad (7)$$

where k_c is the mass transfer coefficient, k_r the reaction rate constant and k is the overall rate constant [19]. Because of the very small particle size of the TiO$_2$ photocatalyst, the chemical reaction rate on the surface is relatively fast, therefore the mass transfer resistance may dominate the overall rate process. Assuming that the specific reaction rate constant is much greater than the mass transfer coefficient:

$$k_r \gg k_c \quad \text{or} \quad \frac{1}{k_r} \ll \frac{1}{k_c} \qquad (8)$$

the overall rate is controlled by the mass transfer resistance:

$$\frac{1}{k} \approx \frac{1}{k_c} \qquad (9)$$

To increase the overall rate of reaction, one can increase the reactant concentration or k_c. Using the correlation of the Schmidt number and the Reynolds number for spherical particle suspensions [19], one can obtain the mass transfer coefficient as

$$k_c = 0.6 \left(\frac{D_{AB}}{d_P} \right) \text{Re}^{1/2} \text{Sc}^{1/3}$$
$$= 0.6 \left(\frac{D_{AB}^{2/3}}{v^{1/6}} \right) \left(\frac{U^{1/2}}{d_P^{1/2}} \right) \qquad (10)$$

where D_{AB} is the diffusion coefficient of the dye molecules in water, d_P the photocatalyst particle diameter, v the kinematic viscosity of water, and U is the velocity of the fluid flowing
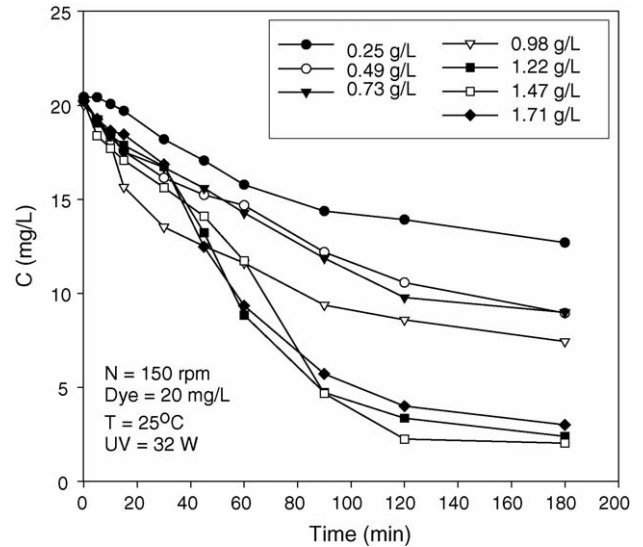
past the particle that is influenced by the agitation speed. Consequently, to increase k_c and thus the overall rate of reaction, one may either decrease the particle size or increase the velocity of the fluid flowing past the particle. From the above reason, as the agitation speed increases, the mass transfer coefficient increase, and the overall dye decomposition rate therefore increases as shown in Fig. 5. For the comparison purpose, we used 150-rpm agitation speed for the other test runs.

3.2. Effect of TiO$_2$ concentration

After understanding the effect of the agitation speed on the dye decomposition kinetics, we used 150-rpm agitation speed to carry out another series of experiments in which the added TiO$_2$ solid concentration was varied from 0.25 to 1.71 g/L. The experimental results at varying TiO$_2$ concentrations are shown in Fig. 6. Similarly, the dye concentrations decrease with time. As shown in Fig. 6, the dye decomposition rate seems to increase with increasing TiO$_2$ concentration up to certain value, then decreases with increasing TiO$_2$ concentration. The initial rates at varying TiO$_2$ concentrations are calculated from the initial slopes and are plotted against the TiO$_2$ concentrations, as shown in Fig. 7. Obviously, the initial rates increase with TiO$_2$ concentration, reach a maximum at 0.98 g/L TiO$_2$, and decrease beyond 0.98 g/L. This can be rationalized in terms of the availability of active sites on TiO$_2$ surface and the light penetration of photoactivating light into the suspension. The availability of the active sites increases with the catalyst concentration in the suspension, but the light penetration decreases with the catalyst concentration in the suspension due to screening effect [20].

In the suspension with diluted TiO$_2$ concentration, the initial reaction rate should be proportional to the number of active sites per unit volume of the solution:

$$-r_0 = k_1[\text{h}^+] \qquad (11)$$

where k_1 is a proportional constant and $[\text{h}^+]$ is the vacancy concentration in the valence band of TiO$_2$. The vacancy
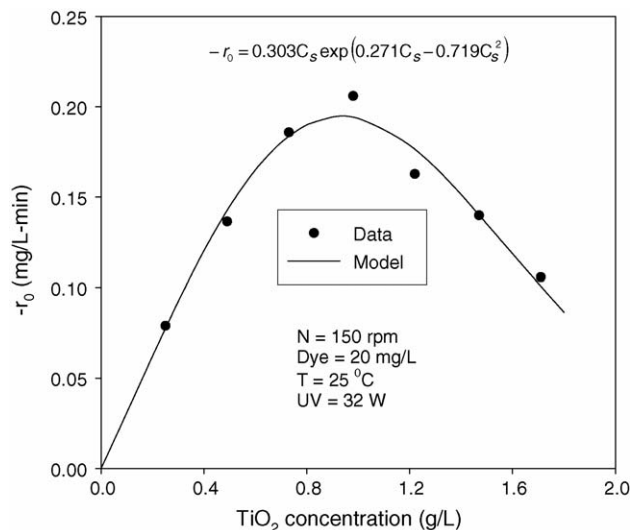
Fig. 7. Effects of TiO$_2$ concentration on the dye initial decomposition rate.

Fig. 8. Effects of initial dye concentration on the dye concentration history.

concentration should be proportional to the energy received by the TiO$_2$ particles and the total surface area of TiO$_2$ that in turn equals the specific surface area (A_S) times the TiO$_2$ suspension concentration (C_S):

$$[h^+] = k_2 E_S A_S C_S \tag{12}$$

The energy received by the TiO$_2$ particles depends on the UV energy intensity and the TiO$_2$ suspension concentration according to the following equation:

$$E_S = k_3 I \exp(-k_4 C_S - k_5 C_S^2) \tag{13}$$

Because the TiO$_2$ suspension concentration is up to 1.71 g/L, the linear relationship of the absorbance with the TiO$_2$ suspension concentration, i.e., the Lambert–Beer's law is not applicable. Using a second-order correlation equation for the absorbance with the TiO$_2$ suspension concentration leads to Eq. (13). Combining Eqs. (11)–(13) leads to

$$-r_0 = k_a C_S \exp(-k_4 C_S - k_5 C_S^2) \tag{14}$$

Eq. (14) was used to fit the experimental initial rates and a non-linear regression method was used to find the best-fit parameters that are shown in Fig. 7. As shown by Fig. 7, Eq. (14) fits the initial dye decomposition rate satisfactorily. Although the 0.98 g/L TiO$_2$ concentration has the highest initial rate, its long-term dye removal efficiency is less than 1.22 g/L as shown in Fig. 6. In order to have a better dye removal efficiency, we used 1.22 g/L TiO$_2$ suspension concentration for the rest of the experimental runs.

3.3. Effect of initial dye concentration

A series of experiments was performed using constant agitation speed 150 rpm, TiO$_2$ suspension concentration 1.22 g/L, 32 W UV lights at 25 °C, but varying initial dye concentrations. The experimental results are shown in Fig. 8. The fractional residual concentration versus time at varying initial dye concentrations is shown in Fig. 9. We can see clearly that the
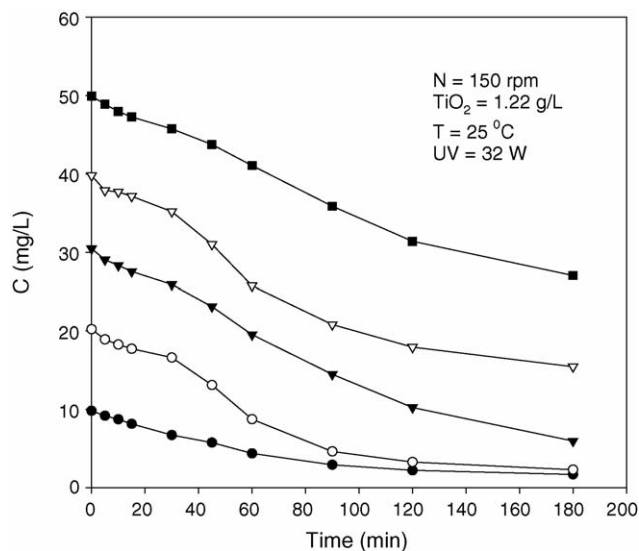
dimensionless residual fraction versus time curves at varying initial dye concentrations do not overlap. This suggests that the reaction kinetics is not first order with respect to the dye concentration. For first-order reactions, the fractional residual concentrations at varying initial reactant concentrations decay exponentially with time only [19,21]:

$$-r_A = -\frac{dC_A}{dt} = kC_A \tag{15}$$

After integrating, the fractional residual concentration can be expressed as

$$\ln \frac{C_A}{C_{A0}} = -kt \quad \text{or} \quad \frac{C_A}{C_{A0}} = \exp(-kt) \tag{16}$$

Eq. (16) suggests that the fractional residual concentration of first-order reactions, decay exponentially with time only, being independent of the initial reactant concentrations [19,21]. The
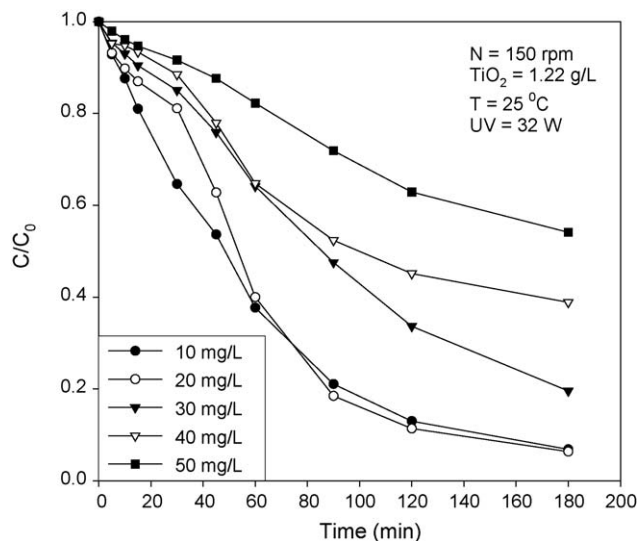

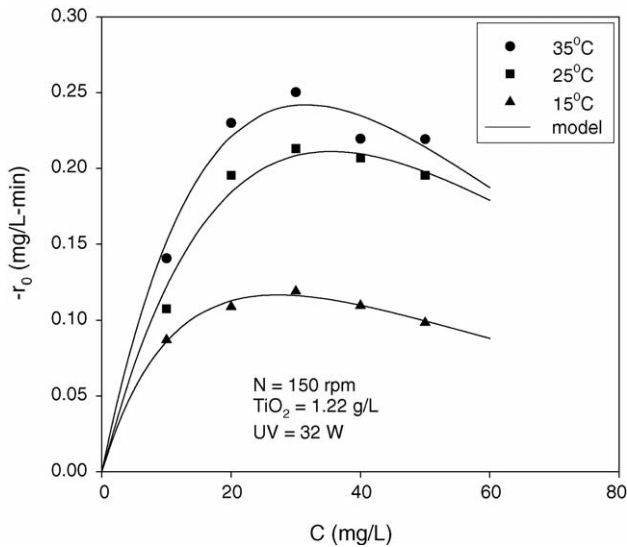Fig. 9. Effects of initial dye concentration on the dye residual fractions.

Fig. 10. Effects of dye concentration on the dye initial decomposition rates at different temperatures.

Fig. 11. Effects of reaction temperature on the dye concentration history.

strong dependence of the fractional residual concentration on the initial dye concentration reveals that the dye decomposition kinetics is not first order with respect to the dye concentration.

The initial rates of dye decomposition at varying initial dye concentrations are calculated from the initial slopes and shown in Fig. 10. As shown by Fig. 10 the initial dye decomposition rate first increases with the initial dye concentration, reaches the maximal value at about 30 mg/L, and then decreases with increasing initial dye concentration. Also shown in Fig. 10 is the predicted curve calculated by the following equation:

$$-r_0 = \frac{k_b C_d \exp(-k_c C_d)}{1 + k_d C_d} \qquad (17)$$

where C_d is the initial dye concentration, k_b the lumped reaction rate coefficient, k_d the dye adsorption equilibrium constant, and k_c is the Lambert–Beer's law coefficient. Eq. (17) is the combination of the Langmuir–Hinshelwood model [22–31] that accounts for the adsorption and reaction of the dye molecule and the Lambert–Beer's law that accounts for the UV energy absorbed by the dye solution. As shown by Fig. 10, Eq. (17) fits the experimental data quite well with the parameters listed in Table 2.

3.4. Effect of temperature

A series of experiments was carried out under the same operating conditions but varying reaction temperatures and the results are shown in Fig. 11 for comparison. As clearly shown by

Fig. 11, the dye decomposition rate increases with the reaction temperature. A higher temperature will give a faster decomposition rate; so we can utilize the heat generated by the UV radiation to heat the reaction solution in practice.

Since the initial rates at 25 °C can be successfully correlated by Eq. (17), we continue to perform two series of experiments to determine the relationships between the initial rates and the initial dye concentration at varying reaction temperatures. The experimental results at 15 and 35 °C are shown in Fig. 12a and
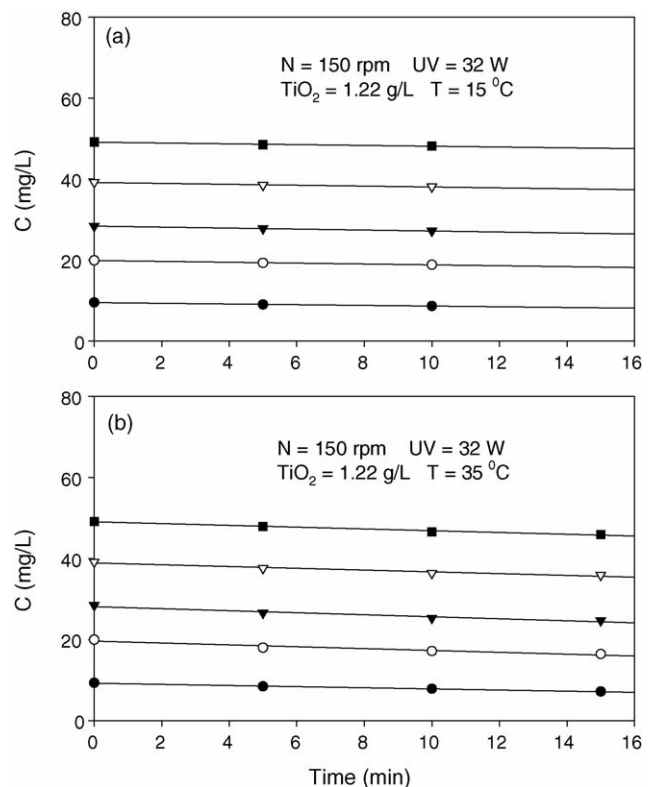

Fig. 12. Effects of initial dye concentration on the dye concentration histories at 15 and 35 °C, respectively.

Table 2
Model parameters to fit the initial dye decomposition rate versus initial dye concentration at varying temperatures

Parameter	15 °C	25 °C	35 °C	Unit
k_b	0.0141	0.0162	0.0208	min^{-1}
k_c	0.0184	0.0282	0.0316	L/mg
k_d	0.0364	4.03E−07	1.05E−12	L/mg

Table 3
The temperature correlation parameters for the rate coefficients

Parameter	For k_b	For k_c	For k_d
A	5.40 min^{-1}	84.79 L/mg	3.12E−164 L/mg
E	14.3 kJ/mol	20.1 kJ/mol	−894.9 kJ/mol

b, respectively. The initial rates of varying initial dye concentrations at 15 and 35 °C are calculated by Eq. (17) and also shown in Fig. 10 for comparison. Table 2 summarizes the model parameters of Eq. (17) for the three reaction temperatures.

The effects of the reaction temperature on the model parameters are shown in Fig. 13. Table 3 summarizes the correlation parameters of the linear plots in Fig. 13 using the following correlation equation:

$$k_i = A_i \exp\left(-\frac{E_i}{RT}\right), \quad i = \text{b, c, d} \tag{18}$$

The physical meaning of the parameter E for k_b represents the activation energy of the dye reaction while that for k_c represents the activation energy of the UV penetration through the dye solution. Both of these two activation energies being positive suggest that a higher temperature favors the dye reaction and UV penetration. The physical meaning of the parameter E for k_d represents the heat of adsorption of the dye molecules onto the TiO$_2$ particles. Like most adsorption processes that are usually exothermic, the negative value of the parameter E for k_d suggests that the dye adsorption onto the TiO$_2$ particles is also exothermic. But unlike most physical adsorption processes that have small adsorption heat, E_d is unreasonably high as shown in Table 3. Perhaps a strong chemical bonding is formed during the dye adsorption onto the TiO$_2$ surface.

3.5. Effect of UV power intensity

Because the dye decomposition is a heterogeneous reaction occurring on the TiO$_2$ particle surface with the active site con-

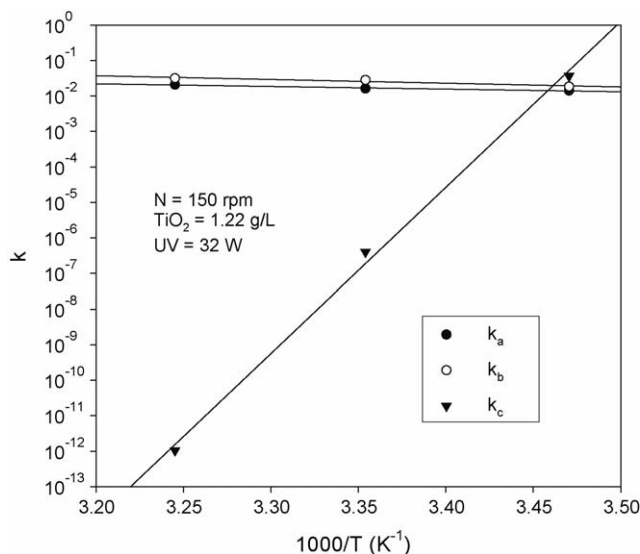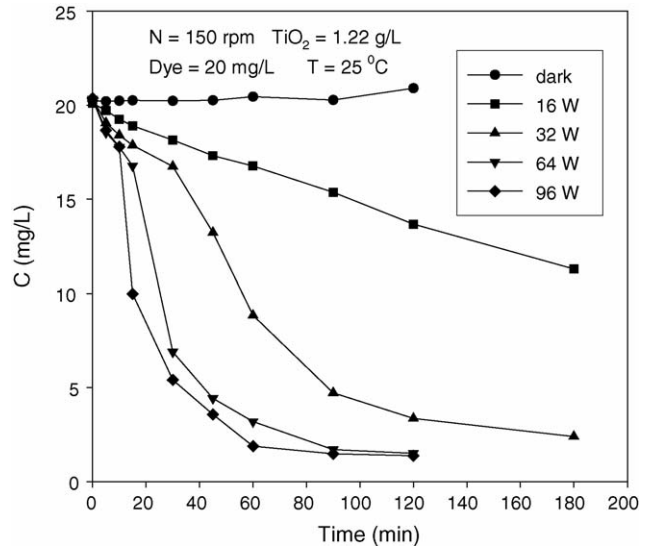Fig. 14. Effects of UV irradiation intensity on the dye concentration history.

centration increasing with the UV energy received, a higher UV power intensity is expected to give a higher decomposition rate. A series of experiments was conducted under the same operating conditions but varying UV power intensities and the results are shown in Fig. 14. Fig. 14 clearly shows that the dye cannot be decomposed without UV irradiation. The initial dye decomposition rates were calculated from the initial slopes and are summarized in Fig. 15 for comparison. As shown by Fig. 15, the initial dye decomposition rate increases with the UV power intensity up to 64 W; for the UV power greater than 64 W, the UV power intensity has little influence on the dye decomposition rate. These results are in agreement with the results of other studies. For example, Ollis et al. [26] stated that at low light intensities, the reaction rate would increase linearly with increasing light intensity (first order), at intermediate light intensities beyond a certain value, the reaction rate would depend on the square root of the light intensity (half order), and at

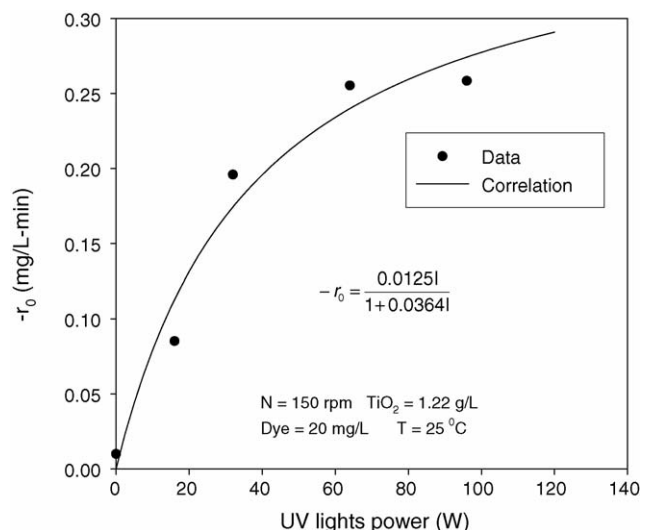Fig. 13. Linear plots of the kinetic model parameters.

Fig. 15. Effects of UV irradiation power intensity on the initial decomposition rate.

high light intensities the reaction rate was independent of the light intensity. In order to quantify the effect of the light intensity on the dye decomposition rate, an equation similar to the Langmuir–Hinshelwood model was used for correlation and the results are shown in Fig. 15.

In summary, the intrinsic dye decomposition kinetics, i.e., without the mass-transfer resistance limitation, can be expressed by the following equation:

$$-r_d = \frac{k_a' C_S C_d \exp(-k_c C_d) \exp(-k_4 C_S - k_5 C_S^2) I}{(1 + k_d C_d)(1 + k_I I)} \tag{19}$$

where k_a' is a lumped rate coefficient.

4. Conclusions

The dye decomposition kinetics by nano-size TiO$_2$ suspension at natural solution pH was experimentally studied by varying the agitation speed, TiO$_2$ suspension concentration, initial dye concentration, temperature, and UV power intensity. From this experimental study, several conclusions can be made:

- The agitation speed, varying from 50 to 200 rpm, has a slight influence on the dye decomposition rate and pH history.
- The dye decomposition rate increases with the TiO$_2$ suspension concentration up to 0.98 g/L, and then decreases with increasing TiO$_2$ suspension concentration. A kinetic model has been developed to successfully correlate the initial rates at varying TiO$_2$ suspension concentrations.
- The initial dye decomposition rate increases with the initial dye concentration up to a certain value depending upon the temperature, and then decreases with increasing initial dye concentration. A kinetic model, based on the Langmuir–Hinshelwood model and the Lambert–Beer's law, has been developed to successfully correlate the initial rates at varying initial dye concentrations.
- In the absence of UV irradiation, the dye cannot be decomposed by the TiO$_2$ suspension. The dye decomposition rate increases with the UV power intensity up to 64 W; the UV power intensity greater than 64 W cannot further increase the dye decomposition rate.

References

[1] R.L.H. Liu, H.-M. Chiu, R.Y.L. Yeh, Int. J. Environ. Stud. 59 (2003) 143.
[2] R. Sanghi, B. Bhattacharya, Water Qual. Res. J. Can. 38 (2002) 553.
[3] M.I. Beydilli, S.G. Pavlostathis, W.C. Tincher, Water Environ. Res. 72 (2000) 698.
[4] S. Liakou, U. Zissi, M. Kornaros, G. Lyberatos, Chem. Eng. Commun. 190 (2003) 645.
[5] B. Van der Bruggen, I. De Vreese, C. Vandecasteele, Ind. Eng. Chem. Res. 40 (2001) 3973.
[6] I. Koyuncu, J. Chem. Tech. Biotechnol. 78 (2003) 1219.
[7] J. Ge, J. Qu, Appl. Catal. B: Environ. 47 (2004) 133.
[8] N.H. Ince, G. Tezcanli, Water Sci. Technol. 40 (1999) 183.
[9] W. Sadik, G. Shama, Process Saf. Environ. Prot. Trans. Inst. Chem. Eng. B 80 (2002) 310.
[10] I. Arslan, I.A. Balcioglu, T. Tuhkanen, J. Environ. Sci. Health A 35 (2000) 775.
[11] J. Peller, K. Vinodgopal, Res. Chem. Intermed. 29 (2003) 307.
[12] N. Daneshvar, D. Salari, A.R. Khataee, J. Photochem. Photobiol. A 157 (2003) 111.
[13] C.M. So, M.Y. Cheng, J.C. Yu, P.K. Wong, Chemosphere 46 (2002) 905.
[14] M. Saquib, M. Muneer, Dyes Pigments 56 (2003) 37.
[15] K. Wang, J. Zhang, L. Lou, S. Yang, Y. Chen, J. Photochem. Photobiol. A 165 (2004) 201.
[16] A. Fujishima, T.N. Rao, D.A. Tryk, J. Photochem. Photobiol. C 1 (2000) 1.
[17] C. Galindo, P. Jacques, A. Kalt, J. Photochem. Photobiol. A 130 (2000) 35.
[18] M.H. Habibi, A. Hassanzadeh, S. Mahdavi, J. Photochem. Photobiol. A 172 (2005) 89.
[19] H.S. Fogler, Elements of Chemical Reaction Engineering, 3rd ed., Prentice Hall, New Jersey, 1999.
[20] I.K. Konstantinou, T.A. Albanis, Appl. Catal. B: Environ. 49 (2004) 1.
[21] O. Levenspiel, Chemical Reaction Engineering, 3rd ed., John Wiley & Sons, New York, 1999.
[22] T. Nguyen, D.F. Ollis, J. Phys. Chem. 88 (1984) 3386.
[23] D.F. Ollis, Environ. Sci. Technol. 19 (1985) 480.
[24] R.W. Matthews, J. Phys. Chem. 91 (1987) 3328.
[25] H. Al-Ekabi, N. Serpone, J. Phys. Chem. 92 (1988) 5726.
[26] D.F. Ollis, E. Pelizzetti, N. Serpone, Sci. Technol. 25 (1991) 1523.
[27] J. Chen, D.F. Ollis, W.H. Rulkens, H. Bruning, Water Res. 33 (1999) 669.
[28] J. Chen, D.F. Ollis, W.H. Rulkens, H. Bruning, Water Res. 33 (1999) 1173.
[29] G. Liu, T. Wu, J. Zhao, H. Hidaka, N. Serpone, Environ. Sci. Technol. 33 (1999) 2081.
[30] J.-K. Yang, A.P. Davis, Environ. Sci. Technol. 34 (2000) 3789.
[31] I.K. Konstantinou, V.A. Sakkas, T.A. Albanis, Water Res. 36 (2002) 2733.